Analytical prediction of stable optical trapping in optical vortices created by three TE or TM plane waves

Tomasz M. Grzegorczyk* **and Jin Au Kong**

Research Laboratory of Electronics, Massachusetts Institute of Technology, 77 Massachusetts Avenue, Cambridge MA 02139, USA

*tomasz.grzegorczyk@mit.edu

Abstract: A closed-form analytical expression of the force on an infinite lossless dielectric cylinder due to multiple plane wave incidences is proposed. The formula for a TE polarization is derived and completes our previous work which was limited to TM polarizations. A unified form of the analytical expression of the force is proposed and used to study the curvature of the one dimensional potential of an optical lattice created by the interference of three plane waves. It is shown that the points of zero curvature yield optical vortices which can be used to stably trap particles of particular sizes and index contrasts with the background. Under these circumstances, the trajectories of the particles can be assimilated to spirals whose centers correspond to the points of undetermined phase in the optical landscape.

OCIS codes: (260.2110) Electromagnetic theory; (020.7010) Trapping; (290.4020) Mie theory

References and links

1. L. Allen, M. W. Beijersbergen, R. J. C. Spreeuw, and J. P. Woerdman, "Orbital angular momentum of light and the transformation of Laguerre-Gaussian laser modes," Phys. Rev. A **45**, 8185–8189 (1992).
2. J. F. Nye and J. V. Hajnal, "The wave structure of monochromatic electromagnetic radiation," Prof. R. Soc. Lond. A **409**, 21–36 (1987).
3. D. G. Grier, "A revolution in optical manipulation," Nature **424**, 810–816 (2003).
4. M. V. Berry, "Optical vortices evolving from helicoidal integer and fractional phase steps," J. Opt. A: Pure Appl. Opt. **6**, 259–268 (2004).
5. L. Paterson, E. Papagiakoumou, G. Milne, V. Garcés-Chávez, S. A. Tatarkova, W. Sibbett, F. J. Gunn-Moore, P. E. Bryant, A. C. Riches, and K. Dholakia, "Light-induced cell separation in a tailored optical landscape," Appl. Phys. Lett. **87**, 123901 (2005).
6. A. Jesacher, S. Fürhapter, C. Maurer, S. Bernet, and M. Ritsch-Marte, "Holographic optical tweezers for object manipulations at an air-liquid surface," Opt. Express **14**, 6342–6352 (2006).
7. K. T. Gahagan and J. G. A. Swartzlander, "Optical vortex trapping of particles," Opt. Lett. **21**, 827–829 (1996).
8. A. Ashkin, J. M. Dziedzic, J. E. Bjorkholm, and S. Chu, "Observation of a single-beam gradient force optical trap for dielectric particles," Opt. Lett. **11**, 288–290 (1986).
9. D. Cojoc, V. Garbin, E. Ferrari, L. Businaro, F. Romanato, and E. Di Fabrizio, "Laser trapping and micro-manipulation using optical vortices," Microelectron. Eng. **78-79**, 125–131 (2005).
10. J. E. Curtis, B. A. Koss, and D. G. Grier, "Dynamic holographic optical tweezers," Opt. Commun. **207**, 169–175 (2002).
11. M. M. Burns, J.-M. Fournier, and J. A. Golovchenko, "Optical Matter: Crystallization and Binding in Intense Optical Fields," Science **249**, 749–754 (1990).
12. J.-M. Fournier, G. Boer, G. Delacrétaz, P. Jacquot, J. Rohner, and R. Salathé, "Building Optical Matter with Binding and Trapping Forces," Proc. SPIE **5514**, 309–317 (2004).

#82201 - $15.00 USD Received 24 Apr 2007; revised 4 Jun 2007; accepted 6 Jun 2007; published 12 Jun 2007

13. T. M. Grzegorczyk and J. A. Kong, "Analytical expression of the force due to multiple TM plane wave incidences on an infinite dielectric cylinder," J. Opt. Soc. Am. B **24**, 644–652 (2006).
14. J. Masajada and B. Dubik, "Optical vortex generation by three plane wave interference," Optics Commun. **198**, 21–27 (2001).
15. B. T. Draine, "The discrete-dipole approximation and its application to interstellar graphite grains," Astrophys. J. **333**, 848–872 (1988).
16. P. C. Chaumet and M. Nieto-Vesperinas, "Coupled dipole method determination of the electromagnetic force on particle over a flat dielectric substrate," Phys. Rev. B **61**, 14119–14127 (2000).
17. T. M. Grzegorczyk, B. A. Kemp, and J. A. Kong, "Stable optical trapping based on optical binding forces," Phys. Rev. Lett. **96**, 113903 (2006).
18. T. M. Grzegorczyk, B. A. Kemp, and J. A. Kong, "Trapping and binding of an arbitrary number of cylindrical particles in an in-plane electromagnetic field," J. Opt. Soc. Am. A **23**, 2324–2330 (2006).
19. D. Maystre and P. Vincent, "Making photonic crystals using trapping and binding optical forces on particles," J. of Opt. A: Pure Appl. Opt. **8**, 1059–1066 (2006).
20. B. A. Kemp, T. M. Grzegorczyk, and J. A. Kong, "Optical momentum transfer to absorbing Mie particles," Phys. Rev. Lett. **97**, 133902 (2006).
21. P. Zemánek, V. Karásek, and A. Sasso, "Optical forces acting on Rayleigh particle placed into interference field," Optics Commun. **240**, 401–415 (2004).
22. A. Ashkin, "Forces of a single-beam gradient laser trap on a dielectric sphere in the ray optics regime," Biophys. J. **61**, 569–582 (1992).

1. Introduction

Laguerre-Gaussian beams have been shown to carry and to transfer orbital momentum to matter [1]. Such beams are characterized by a helical phase structure and a zero intensity at their center due to the destructive interference close to the vortex phase singularity [2, 3, 4]. These properties have allowed for the recent creation of microfluidic devices such as sorting devices, mixers, and pumps [5, 6], and have been able to trap low index particles [7], as an extension of the more traditional optical tweezer based on Gaussian beams [8]. In practice, Laguerre-Gaussian beams are typically realized using diffractive optical elements or computer-generated holograms [7, 9] from which single and multiple-particle traps have been realized, as already shown experimentally [10]. Independently, multiple particle trapping has also been demonstrated using three interfering beams which create an hexagonal pattern of high intensity regions [11, 12]. This simple configuration has been shown to trap hundreds of particles, typically in the high field regions.

In this paper we show that, independently of the polarization, the simple three-beam interference pattern exhibits a phase singularity which can be used to trap properly designed particles in a spiral-like fashion when the curvature of the optical pseudo-potential is close to zero (we denote by pseudo-potential the potential-like function along the $\hat{x}$ direction obtained from the force). In order to show this, we first derive a closed-form analytical expression of the force on an infinite lossless dielectric cylinder subject to multiple TE (magnetic field parallel to the axis of the cylinder) plane waves. This derivation completes our previous work [13] where the general framework of the computation was laid out but only carried through for the TM polarization. We show here that the forces due to TE or TM incidences are written in a similar way, in which the polarization dependent coefficients do not affect the qualitative form of the force. With this conclusion, we proceed by analytically computing the curvature of the pseudo-potential and showing that close to its zero, the optical landscape creates a force field that induces spiral-like motions of particles, centered at the points of undetermined phases also called optical vortices [14]. By analyzing the forces, we establish the threshold in particle size between an outward spiraling motion and an inward spiraling motion, the latter yielding a stable trap at the optical vortex.

#82201 - $15.00 USD Received 24 Apr 2007; revised 4 Jun 2007; accepted 6 Jun 2007; published 12 Jun 2007

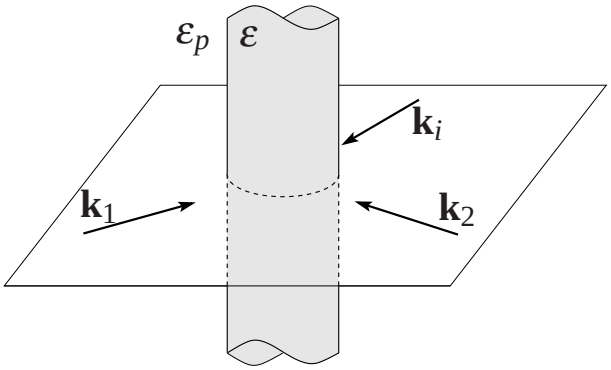

Fig. 1. Configuration of the problem: an infinitely long cylinder of permittivity ε_p is embedded in a background of permittivity ε and is subject to multiple in-plane incidences.

2. Analytical expression of the force

The framework of the problem under consideration is represented in Fig. 1: multiple plane waves of similar amplitude and incident angles $(\theta = \pi/2, \phi)$ impinge on an infinite lossless dielectric cylinder of radius a and permittivity ε_p, in a background medium of permittivity ε. The interference of the multiple in-plane incidences creates an optical landscape which in turn induces a force on the cylindrical particle. This force has so far been computed either numerically using techniques such as the discrete-dipole approximation [15, 16], or semi-numerically using an analytical expansion of the fields but a numerical evaluation of the integral in the Maxwell stress tensor formulation [17, 18, 19, 20]. Although not immediately straightforward, however, a series of algebraic manipulations can be performed on the force expression obtained from the Maxwell stress tensor, using an expansion of the electromagnetic fields in the cylindrical coordinate system. An overview of the method along with some mathematical details have been presented in [13]: a generic formula for the force has been obtained for both TE and TM incidences, and further simplifications were performed to reduce the TM formula to a closed-form expression from which physical conclusions were drawn. The first purpose of this paper is to generalize the closed-form formula to the TE case as well. In order to do this, we rewrite without further details the generic formula of the force due to a single plane wave first (the generalization to multiple waves follows), as obtained in [13, Eq. (16a)]:

$$\begin{aligned}
\mathbf{F}^{TE} = {} & \hat{x}\frac{a\pi\varepsilon}{2}\Re\left(\sum_{\mathsf{n}}\left(\frac{\mathsf{n}(\mathsf{n}+1)}{(ka)^2}-1\right)H_{z_\mathsf{n}}H^*_{z_{\mathsf{n}+1}} - E_{\phi_\mathsf{n}}E^*_{\phi_{\mathsf{n}+1}}\right) \\
& + \hat{y}\frac{a\pi\varepsilon}{2}\Im\left(\sum_{\mathsf{n}}\left(\frac{\mathsf{n}(\mathsf{n}+1)}{(ka)^2}-1\right)H_{z_\mathsf{n}}H^*_{z_{\mathsf{n}+1}} - E_{\phi_\mathsf{n}}E^*_{\phi_{\mathsf{n}+1}}\right) \\
& + \hat{x}\frac{\pi\varepsilon}{2k}\Re\left(\sum_{\mathsf{n}}\mathsf{n}H_{z_\mathsf{n}}(E^*_{\phi_{\mathsf{n}+1}} - E^*_{\phi_{\mathsf{n}-1}})\right) \\
& - \hat{y}\frac{\pi\varepsilon}{2k}\Im\left(\sum_{\mathsf{n}}\mathsf{n}H_{z_\mathsf{n}}(E^*_{\phi_{\mathsf{n}+1}} + E^*_{\phi_{\mathsf{n}-1}})\right), \qquad (1)
\end{aligned}$$

#82201 - $15.00 USD Received 24 Apr 2007; revised 4 Jun 2007; accepted 6 Jun 2007; published 12 Jun 2007

where

$$E_{\phi_n} = k\left[a_n^{(M)s} H_n^{(1)'}(k\rho) + a_n^{(M)} J_n'(k\rho)\right] \tag{2a}$$

$$H_{z_n} = k\left[a_n^{(M)s} H_n^{(1)}(k\rho) + a_n^{(M)} J_n(k\rho)\right] \tag{2b}$$

$$a_n^{(M)} = \frac{i^{n+1} e^{-in\phi_i}}{k} E_{hi}\,, \tag{2c}$$

E_{hi} is the amplitude of the incident wave of wave vector k and incident angle ϕ_i, $H_n^{(1)}$ and J_n are the Hankel and Bessel functions, respectively, and the prime denotes a derivative with respect to the argument. The coefficients $a_n^{(M)s}$ are related to $a_n^{(M)}$ by the T_n^M coefficients of a cylinder [13, Eq. (5b)].

Although (1) provides an exact relation to compute the force on a lossless dielectric cylinder under TE illumination, it does not provide an intuitive physical understanding of momentum transfer to particles. We therefore simplify (1) further by replacing the expression of $a_n^{(M)s}$ into Eqs. (2) and using the Wronskian to obtain

$$E_{\phi_n} = \frac{2k}{i\pi a}\frac{J_n'(k_p a)}{D_n^{TE}}\,, \qquad\qquad H_{z_n} = \frac{2k_p}{i\pi a}\frac{J_n(k_p a)}{D_n^{TE}}\,, \tag{3}$$

where k_p is the wave vector inside the particle and D_n^{TE} is given by

$$D_n^{TE} = kH_n^{(1)}(ka)J_n'(k_p a) - k_p H_n^{(1)'}(ka)J_n(k_p a)\,. \tag{4}$$

Inserting Eqs. (3) into (1) and extracting the $\hat{x}$ component of the force, we write $F_x^{TE} = (\pi\varepsilon/2)\Re(A+B)$ where, after some algebra,

$$\begin{aligned} A = & -\left(\frac{2}{\pi a}\right)^2 \frac{i}{k^2}|E_{hi}|^2 \sum_n \frac{e^{i\phi_i}}{D_n^{TE} D_{n+1}^{TE^*}} \times \\ & \left[\left(\left(\frac{k_p^2}{k^2} + \frac{k^2}{k_p^2}\right)\frac{n(n+1)}{a} - k_p^2 a + k^2 a\right) J_n(k_p a) J_{n+1}(k_p a) \right. \\ & \left. - \frac{k^2}{k_p}(n+1)J_{n+1}^2(k_p a) - \frac{k^2}{k_p} n J_n^2(k_p a)\right] \end{aligned} \tag{5a}$$

$$\begin{aligned} B = & -\left(\frac{2}{\pi a}\right)^2 \frac{i}{k^2}|E_{hi}|^2 \sum_n \left[e^{i\phi_i}\frac{k_p n J_n^2(k_p a)}{D_n^{TE} D_{n+1}^{TE^*}}\right. \\ & - e^{-i\phi_i}\frac{k_p(n+1)J_{n+1}^2(k_p a)}{D_n^{TE^*} D_{n+1}^{TE}} + \frac{n(n+1)}{a} J_n(k_p a) J_{n+1}(k_p a) \times \\ & \left.\left(\frac{e^{-i\phi_i}}{D_n^{TE^*} D_{n+1}^{TE}} - \frac{e^{i\phi_i}}{D_n^{TE} D_{n+1}^{TE^*}}\right)\right] \end{aligned} \tag{5b}$$

The force is obtained by adding Eqs. (5a) to (5b) and taking the real part. Details of the algebraic manipulations are provided in the appendix, after which the force is simplified into the

#82201 - $15.00 USD Received 24 Apr 2007; revised 4 Jun 2007; accepted 6 Jun 2007; published 12 Jun 2007

expression:

$$\mathbf{F}^{TE} = \hat{k}_i \frac{4\varepsilon}{\pi a} \frac{k_p^2 - k^2}{k^2} |E_{hi}|^2 \sum_0^{+\infty} \Im\left(D_{\mathsf{n}}^{TE*} D_{\mathsf{n}+1}^{TE}\right) \times \frac{\frac{\mathsf{n}(\mathsf{n}+1)}{(ka)^2} J_{\mathsf{n}}(k_p a) J_{\mathsf{n}+1}(k_p a) + J'_{\mathsf{n}}(k_p a) J'_{\mathsf{n}+1}(k_p a)}{|D_{\mathsf{n}}^{TE}|^2 \, |D_{\mathsf{n}+1}^{TE}|^2} \tag{6}$$

for a single plane wave ($\hat{k}_i = \mathbf{k}_i/|\mathbf{k}_i|$), and

$$\mathbf{F}_{ij}^{TE} = (\hat{x}\cos\Phi_{ij} + \hat{y}\sin\Phi_{ij}) \frac{4\varepsilon}{\pi a} \frac{k_p^2 - k^2}{k^2} |E_{hi}|^2 \sum_0^{+\infty} \Im\left(D_{\mathsf{n}}^{TE*} D_{\mathsf{n}+1}^{TE} e^{-\mathrm{i}(\mathsf{n}+0.5)(\phi_i - \phi_j)}\right) \times \frac{\frac{\mathsf{n}(\mathsf{n}+1)}{(ka)^2} J_{\mathsf{n}}(k_p a) J_{\mathsf{n}+1}(k_p a) + J'_{\mathsf{n}}(k_p a) J'_{\mathsf{n}+1}(k_p a)}{|D_{\mathsf{n}}^{TE}|^2 \, |D_{\mathsf{n}+1}^{TE}|^2} \tag{7}$$

for the interaction between plane wave #i and #j, where $\Phi_{ij} = (\mathbf{k}_i - \mathbf{k}_j)\cdot\rho + (\phi_i + \phi_j)/2$. Naturally, (7) reduces to (6) when $i = j$ in a straightforward manner.

A comparison between (7) for the TE polarization and [13, Eq. (27)] for the TM polarization reveals that the two formulae are fundamentally similar, with only a few polarization dependent coefficients. Unifying the two expressions, we write the total force for a given polarization (p) as

$$F^{(p)} = \sum_{i,j=1}^{M} F_{ij}^{(p)}, \tag{8a}$$

$$F_{ij}^{(p)} = e^{\mathrm{i}\Phi_{ij}} K^{(p)} \sum_{\mathsf{n}=0}^{+\infty} \Lambda^{(p)} \Im\left(\gamma_{\mathsf{n}}^{(p)} \beta_{\mathsf{n}}\right), \tag{8b}$$

where

$$K^{(p)} = \frac{4\varepsilon}{\pi a} \frac{k_p^2 - k^2}{k^2} |E^{(p)}|^2, \tag{9a}$$

$$\Phi_{ij} = (\mathbf{k}_i - \mathbf{k}_j)\cdot\rho + \frac{\phi_i + \phi_j}{2}, \tag{9b}$$

$$\beta_{\mathsf{n}} = e^{-\mathrm{i}(\mathsf{n}+0.5)(\phi_i - \phi_j)}, \tag{9c}$$

$$\gamma_{\mathsf{n}}^{(p)} = D_{\mathsf{n}}^{(p)*} D_{\mathsf{n}+1}^{(p)}, \tag{9d}$$

$$\Lambda^{TM} = \frac{J_{\mathsf{n}}(k_p a) J_{\mathsf{n}+1}(k_p a)}{|D_{\mathsf{n}}^{TM}|^2 \, |D_{\mathsf{n}+1}^{TM}|^2}, \tag{9e}$$

$$\Lambda^{TE} = \frac{\frac{\mathsf{n}(\mathsf{n}+1)}{(ka)^2} J_{\mathsf{n}}(k_p a) J_{\mathsf{n}+1}(k_p a) + J'_{\mathsf{n}}(k_p a) J'_{\mathsf{n}+1}(k_p a)}{|D_{\mathsf{n}}^{TE}|^2 \, |D_{\mathsf{n}+1}^{TE}|^2}, \tag{9f}$$

$$D_{\mathsf{n}}^{TM} = kH_{\mathsf{n}}^{(1)'}(ka) J_{\mathsf{n}}(k_p a) - k_p H_{\mathsf{n}}^{(1)}(ka) J'_{\mathsf{n}}(k_p a), \tag{9g}$$

$$D_{\mathsf{n}}^{TE} = kH_{\mathsf{n}}^{(1)}(ka) J'_{\mathsf{n}}(k_p a) - k_p H_{\mathsf{n}}^{(1)'}(ka) J_{\mathsf{n}}(k_p a). \tag{9h}$$

The symbols in Eqs. (9) are defined as follows: ρ is the position of the particle in the (xy) plane, (p) =TE, TM indicates the polarization, $E^{(p)}$ is the amplitude of the incident polarization,

#82201 - $15.00 USD Received 24 Apr 2007; revised 4 Jun 2007; accepted 6 Jun 2007; published 12 Jun 2007

while ($\mathbf{k}_i$, ϕ_i) and ($\mathbf{k}_j$, ϕ_j) are the two wavevectors and incident angles of the two plane waves with $|\mathbf{k}_i| = |\mathbf{k}_j| = k = k_0\sqrt{\varepsilon}$, $k_p = k_0\sqrt{\varepsilon_p}$, $k_0 = 2\pi/\lambda$. Under the notation of (8), the x and y components of the force are given by $F_{x_{ij}}^{(p)} = \Re(F_{ij}^{(p)})$ and $F_{y_{ij}}^{(p)} = \Im(F_{ij}^{(p)})$, where $\Re(\cdot)$ and $\Im(\cdot)$ denote the real and imaginary part operators, respectively.

It is important to emphasize that (8) is a fundamental relation which is straightforward to evaluate and which gives the force on a cylinder with no approximation. In addition, it immediately demonstrates a series of known results, previously established either experimentally or analytically using some approximations (typically a Rayleigh approximation when particles are very small [21] or a ray optics approximation when they are large compared to the wavelength [22]): in the case of a single incidence ($F^{(p)} = F_{ii}^{(p)}$), the force is in the same direction as the incident wave, the force vanishes if there is no permittivity contrast, it is always positive and pushing the particle; in the case of a Gaussian beam (written as a superposition of weighted plane waves), the operating mode of an optical tweezer can be demonstrated and more generally, the longitudinal and transverse forces can be shown to be separately controlled by the size and the permittivity contrast, respectively [13]. In addition, the polarization dependent coefficients in (8) can be assimilated to simple constants: they do not influence the qualitative dependence of the force on the various incident waves or on the position in space ρ. The subsequent study on the pseudo-potential is therefore in essence identical for both TE or TM polarizations.

3. Pseudo-potential and zero curvature points

In addition to providing a closed-form expression of the force, (8) provides a way to study the pseudo-potential (along the $\hat{x}$ direction) created by the interference of three plane waves in an analytical manner. The plane waves are supposed to have identical amplitudes and their wavevectors are separated by an angle of $2\pi/3$, yielding an hexagonal interference pattern of high and low intensity regions. These regions can either attract or repel particles, as function of their size and permittivity contrast compared to the background medium. The attraction or repulsion can be quantitatively studied by analyzing the curvature of the pseudo-potential, obtained by a simple derivative of (8) with respect to x, which can be here obtained analytically. This process is simplified by combining the symmetric force terms as

$$F_{ij}^{(p)} + F_{ji}^{(p)} = 2K^{(p)} e^{\mathrm{i}(\phi_i+\phi_j)/2} \sum_{\mathsf{n}=0}^{+\infty} \Lambda^{(p)} \left[\Re(\alpha)\Re(\beta_\mathsf{n})\Im(\gamma_\mathsf{n}^{(p)}) + \mathrm{i}\Im(\alpha)\Im(\beta_\mathsf{n})\Re(\gamma_\mathsf{n}^{(p)}) \right]. \tag{10}$$

The curvature of the pseudo-potential can be obtained from

$$\frac{\partial^2 U^{(p)}}{\partial x^2} = -\frac{\partial F^{(p)}}{\partial x}, \tag{11}$$

which yields:

$$\frac{\partial^2 U^{(p)}}{\partial x^2} = -2\mathrm{i}k_{ij_x} K^{(p)}\, e^{\mathrm{i}(\phi_i+\phi_j)/2} \sum_{i=1}^{2} \sum_{j=i+1}^{3} \sum_{\mathsf{n}=0}^{+\infty} \Lambda^{(p)} \cdot \left[\cos(\mathbf{k}_{ij}\cdot\rho)\Im(\beta_\mathsf{n})\Re(\gamma_\mathsf{n}^{(p)}) + \mathrm{i}\sin(\mathbf{k}_{ij}\cdot\rho)\Re(\beta_\mathsf{n})\Im(\gamma_\mathsf{n}^{(p)}) \right] \tag{12}$$

where $k_{ij_x} = (\mathbf{k}_i - \mathbf{k}_j)\cdot\hat{x}$. A positive (negative) curvature yields a stable (unstable) trap due to a pseudo-potential well (mountain). Various curvatures as function of particle size are shown

#82201 - $15.00 USD Received 24 Apr 2007; revised 4 Jun 2007; accepted 6 Jun 2007; published 12 Jun 2007

in Fig. 2 for both TE and TM polarizations, at two highly symmetric locations in the lattice: $\rho_0 = (0,0)$ and $\rho_1 = (2\lambda/(3\sqrt{3\varepsilon}),0)$, the latter point being denoted by the right-most cross in Fig. 3 and corresponding to a phase singularity as we shall illustrate hereafter. Although Fig. 2 only shows the curvature along the x direction, which is not sufficient to conclude on the efficiency of the two-dimensional trapping at either ρ_0 or ρ_1, it is straightforward to extend the study to other directions and unambiguously characterize the trapping properties in two dimensions. It can be seen from Fig. 2 that at the origin, the curvature is positive for small particles under a TM illumination. This is a direct illustration of the fact that small dielectric particles are well trapped in high intensity regions due to the gradient force, as it has already been demonstrated multiple times using the Rayleigh approximation. Interestingly, the same particles are not stably trapped in the high intensity regions for a TE polarization (note that the optical landscape refers to the magnetic field in this case). A dual behavior occurs at ρ_1 for both polarizations.

The oscillating nature of the curve indicates that the stable and unstable equilibria alternate as the particle size increases, with the first crossing points located at $a \simeq 0.2264\lambda$ for the TM incidence and $a \simeq 0.2105\lambda$ for the TE incidence. The locations of these crossing points can be approximated by realizing that for small particles, the sole $\mathsf{n} = 0$ term in (8) suffices to obtain a good approximation of the force [13]. A zero curvature coincides in this case with the first zero of $J_0(k_p a)$ for the TM polarization ($k_p a \simeq 2.405$), and the first zero of $J_1'(k_p a)$ for the TE polarization ($k_p a \simeq 1.841$). Using the numerical values given in the caption of Fig. 2, the two zeros yield $a = 0.239\lambda$ for TM and $a = 0.183\lambda$ for TE. The disagreement with the exact values stems from the fact that such sizes of particles are not very small compared to the wavelength so that the approximation of using only the $\mathsf{n} = 0$ term is less accurate.

Using (8), it can be easily demonstrated that the crossing points (and in fact the whole curve at ρ_0 presented in Fig. 2) are independent of frequency if the electrical size of the particle remains unchanged, *i.e.* $k_0 a =$ constant: at the origin the sine term vanishes and the cosine term reduces to unity while the other dependencies are $K^{(p)} \sim k_0$, $\Lambda^{(p)} \sim 1/k_0^4$, and $\gamma_{\mathsf{n}}^{(p)} \sim k_0^2$. With the additional k_{ij_x} term, $\partial^2 U^{(p)}/\partial x^2$ becomes independent of frequency at ρ_0. This property allows us to make a connection with the results presented in [18, Fig. 3], where the attraction and repulsion of the high intensity regions was clearly illustrated for a TM incidence and particle sizes of $a = 0.15\lambda$ and $a = 0.3\lambda$, respectively, although the results were obtained at a different wavelengths. The previous argument can be generalized to the location ρ_1 to show that in this case, only the crossing points in Fig. 2 are independent of frequency.

fig.curv also provides the basis to study the trapping efficiency of a given particle in the optical lattice, which is often a concern in experiments. The best trapping efficiency at ρ_0 is obtained when the curvature of the corresponding pseudo-potential well is positive and maximum, which corresponds to the positive maxima of the solid (dashed) curves for the TM (TE) polarization. The first such sizes are $a \simeq 0.142\lambda$ and $a \simeq 0.293\lambda$ for a TM and TE incidence, respectively. Not only these points correspond to the steepest well at ρ_0 but they also correspond to the steepest mountain at ρ_1, thus combining the best attraction by the high intensity regions to the best repulsion by the low intensity regions. Correspondingly, it is also possible to trap in the low intensity regions by selecting the negative extrema at ρ_0 or the positive extrema at ρ_1. In two dimensions, however, this trapping is not symmetric because of the asymmetry of the three incident waves so that the pseudo-potential well is steeper in some directions than in others (data not shown for brevity).

Finally, we emphasize the importance of the points of zero curvature in Fig. 2, which correspond to a flat pseudo-potential at both ρ_0 and ρ_1. The force distribution for a TM polarization at $a = 0.2264\lambda$ (the first crossing point) is illustrated by the arrows on the right side of Fig. 3, while the background represent the incident intensity. It is clearly seen that neither the high in-

#82201 - $15.00 USD Received 24 Apr 2007; revised 4 Jun 2007; accepted 6 Jun 2007; published 12 Jun 2007

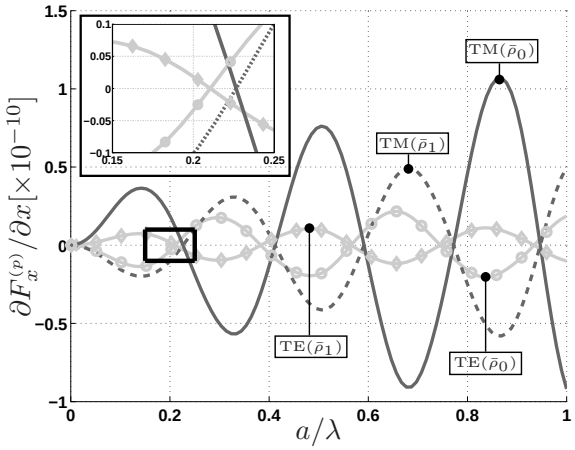

Fig. 2. Curvature of the pseudo-potential along the $\hat{x}$ axis at $\rho_0 = (0,0)$ and $\rho_1 = (2\lambda/(3\sqrt{3\varepsilon}),0)$a ($\rho_0$ corresponds to the point of maximum field intensity while ρ_1, shown by the right-most '+' sign in Fig. 3, corresponds to the point of minimum field intensity). The incident field is obtained from three plane waves of equal amplitude and directions separated by $2\pi/3$, either TE or TM polarized. The inset depicts a zoomed version of the black rectangle and shows the identical crossing points for the respective polarizations. Other parameters: $\lambda = 1064$ nm, $\varepsilon = 1.69\varepsilon_0$, $\varepsilon_p = 2.56\varepsilon_0$.

tensity regions nor the low intensity regions are attractive or repulsive, but that optical vortices are formed around ρ_1. The left side of Fig. 3 shows the phase of the field, where singularities are clearly seen at ρ_1 symmetry points, yielding optical vortices. These vortices, however, are only effective at trapping particles if the curvature of the pseudo-potential is close to zero, as we show subsequently.

A vortex trapping occurs at ρ_1 when the phase singularity points induce an attractive force on the particle. This can be quantified by looking at a circle centered at ρ_1 and requiring the force in the normal direction to be pointing inward (toward ρ_1). Such a circle is represented in Fig. 3, with a radius arbitrarily chosen of 140 nm, along which we compute the force and the normal component as $\hat{F}^{TM} \cdot \hat{n}$ where $\hat{n}$ is the outward pointing normal vector to the circle. A positive (negative) value of the dot product indicates a normal force pointing away from (toward) ρ_1, the negative value yielding a spiral-like attractor. The results are presented in Fig. 4 for two sizes of particles. The first one corresponds to the zero curvature of the pseudo-potential, *i.e.* $a = 0.2264\lambda$, and shows that various locations around the circle experience different directions of normal force. Such configuration is therefore not adequate for an inward spiraling motion, and a larger size of particle needs to be chosen (a smaller size would yield a less attractive ρ_1 point). The minimum value obtained for which the dot product is always negative all around the circle is $a = 0.243\lambda$, which is the second curve shown in Fig. 4. The motion corresponding to these two sizes of particles is illustrated in Fig. 3. The first trajectory (marked '1') corresponds to $a = 0.2264\lambda$ and is seen to spiral away from the singular phase points. Eventually, the particle takes a triangular path between the three closest high intensity points, exactly following the force flow shown on the right side of Fig. 3. Although theoretically the particle can be trapped at ρ_0, Brownian motion will prevent such a trapping to occur in experiments. The second trajectory illustrated in Fig. 3 (marked '2') corresponds to $a = 0.243\lambda$. As predicted in Fig. 4, the normal

#82201 - $15.00 USD Received 24 Apr 2007; revised 4 Jun 2007; accepted 6 Jun 2007; published 12 Jun 2007

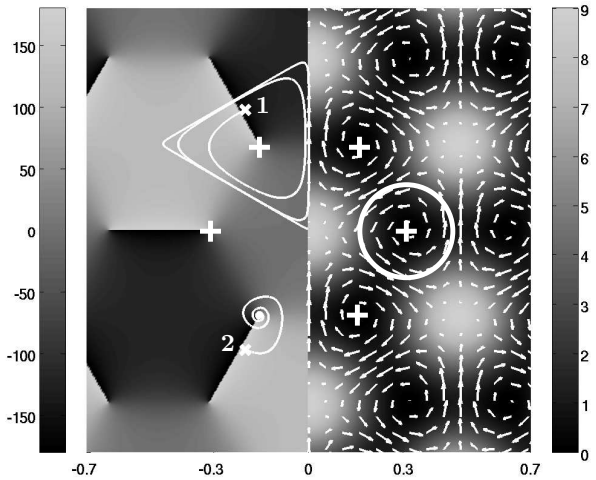

Fig. 3. Background pattern left: phase of the incident electric field (in degrees). Background pattern right: incident TM intensity distribution (in V^2/m^2). Arrows (symmetric in x, only $x > 0$ is shown for clarity): force on a particle with parameters $a = 0.2264\lambda$, $\lambda = 1064$ nm, $\varepsilon = 1.69\varepsilon_0$, $\varepsilon_p = 2.56\varepsilon_0$. The '+' signs indicate the minimum field intensity points corresponding to possible optical vortices (the right-most sign corresponds to ρ_1). Trajectory '1' corresponds to a particle with $a = 0.243\lambda$ starting at $(-200\text{ nm}, 380\text{ nm})$ (denoted by the '$\times$' sign), and shows that the particle is not trapped by the landscape. Trajectory '2' corresponds to a particle with $a = 0.2264\lambda$ starting at $(-200\text{ nm}, -380\text{ nm})$ (denoted by the '$\times$' sign), and shows that the particle is trapped by the landscape in a spiral-like manner. Dimensions along the horizontal axes are given in μm and the two axes are equal.

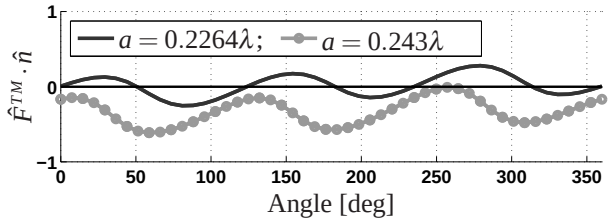

Fig. 4. Normalized normal component of the force along the white circle (centered around ρ_1) for two sizes of particles. The always negative values for $a = 0.243\lambda$ indicate that the normal force is always attracting the particle toward ρ_1, yielding a spiral attractor.

#82201 - $15.00 USD Received 24 Apr 2007; revised 4 Jun 2007; accepted 6 Jun 2007; published 12 Jun 2007

force is here always attractive resulting in an inward spiral-like motion toward the point of low intensity (a symmetric point to ρ_1), resulting in a stable trap. The final position exactly corresponds to the phase singular point, as predicted.

4. Conclusion

The main contribution of this paper is to provide an analytical framework for the study of the pseudo-potential due to multiple plane waves incident on a lossless cylindrical dielectric particle. In this regard, we have generalized the work proposed in [13] in two main aspects. The first has been to provide an analytic expression of the force for a TE incidence, in addition to the TM incidence already known. The second aspect has been to study the curvature of the pseudo-potential generated by three plane waves, which has allowed us to provide a deeper analysis of the trapping results obtained in earlier works. As a result, we have predicted the formation of periodic force vortices in the optical landscape, which induce spiral-like trajectories of particles whose parameters yield points close to the zeros of the pseudo-potential. As function of their parameters (size and index contrast with the background medium), the particles following these trajectories have been shown to be either trapped at the location of the optical vortices, or to be permanently moving between three intensity maxima. These phenomena are shown here to occur at particle sizes of about 0.2λ, but quantitatively similar results are obtained at sizes corresponding to the other zeros of the pseudo-potential in Fig. 2, at about 0.4λ, 0.6λ, etc. Since these crossing points correspond to increasing particle size, they yield configurations that are less and less sensitive to Brownian motion and more appropriate for experimental verifications.

This work is sponsored by NASA-USRA under Contracts No. NAS5-03110 and No. 07605-003-055, by the Department of the Air Force under Air Force Contract No. FA8721-05-C-0002.

Appendix

We provide here a few algebraic details to simplify Eqs. (5a) and (5b) into (7). The first step is to generalize Eqs. (5a) and (5b) to take multiple incidences into account. This is simply done by the transformation

$$e^{\mathrm{i}\phi_i} \longrightarrow e^{-\mathrm{i}\mathsf{n}\phi_i}\, e^{\mathrm{i}(\mathsf{n}+1)\phi_j}\,, \tag{13}$$

where ϕ_i and ϕ_j are the angles of incidence of two plane waves, the total force being obtained by adding all (i,j) contributions. In addition, the space dependency $\exp(\mathrm{i}\mathbf{k}_i\cdot\rho)$ is also added to each $a_{\mathsf{n}}^{(M)}$ coefficient. The equations become

$$\begin{aligned} A = & \left(\frac{2}{\pi a}\right)^2 \frac{2a}{k^2}|E_{hi}|^2 e^{(\phi_i+\phi_j)/2} \sum_{\mathsf{n}=0}^{+\infty} \frac{1}{|D_{\mathsf{n}}^{TE}|^2 D_{\mathsf{n}+1}^{TE}|^2} \times \\ & \left[\frac{\mathsf{n}(\mathsf{n}+1)}{(ka)^2} k_p^2 J_{\mathsf{n}} J_{\mathsf{n}+1} - (k_p^2 J_{\mathsf{n}} J_{\mathsf{n}+1} + k^2 J'_{\mathsf{n}} J'_{\mathsf{n}+1})\right] \times \\ & \Im\left(D_{\mathsf{n}}^{TE^*} D_{\mathsf{n}+1}^{TE} e^{-\mathrm{i}(\mathsf{n}+0.5)(\phi_i-\phi_j)}\right), \end{aligned} \tag{14a}$$

$$\begin{aligned} B = & -\left(\frac{2}{\pi a}\right)^2 \frac{2\mathrm{i}k_p}{k^2}|E_{hi}|^2 \cos\left(\frac{\phi_i+\phi_j}{2}\right) \times \\ & \sum_{\mathsf{n}} \frac{e^{-\mathrm{i}(\mathsf{n}+0.5)(\phi_i-\phi_j)}}{D_{\mathsf{n}}^{TE} D_{\mathsf{n}+1}^{TE^*}} \mathsf{n} J_{\mathsf{n}} J'_{\mathsf{n}+1}\,, \end{aligned} \tag{14b}$$

where it is understood that the argument of the Bessel functions is $k_p a$ (*i.e.* $J_{\mathsf{n}} \equiv J_{\mathsf{n}}(k_p a)$). Further simplifications require the conversion of the sums to have the same limits (a sum from $\sum_{\mathsf{n}} = \sum_{\mathsf{n}=-\infty}^{+\infty}$ is converted to $\sum_{\mathsf{n}=0}^{+\infty}$ by adding the symmetric terms $(\mathsf{n}, -\mathsf{n}-1)$ and conversely),

#82201 - $15.00 USD Received 24 Apr 2007; revised 4 Jun 2007; accepted 6 Jun 2007; published 12 Jun 2007

the proper combination of terms from (14a) and (14b), and the use of identities on the derivative of the Bessel functions. We finally obtain (for a single incidence for example):

$$A = -\left(\frac{2}{\pi a}\right)^2 \frac{\mathrm{i}a}{k^2}|E_{hi}|^2 e^{\mathrm{i}\phi_i} \times \sum_{\mathrm{n}} \frac{1}{D_{\mathrm{n}}^{TE^*} D_{\mathrm{n}+1}^{TE}} \left[\left(\frac{\mathrm{n}(\mathrm{n}+1)}{(ka)^2} - 1\right) k_p^2 J_{\mathrm{n}} J_{\mathrm{n}+1} - k^2 J'_{\mathrm{n}} J'_{\mathrm{n}+1}\right] \tag{15a}$$

$$B = -\left(\frac{2}{\pi a}\right)^2 \frac{2\mathrm{i}k_p}{k^2}|E_{hi}|^2 \cos\phi_i \sum_{\mathrm{n}} \frac{\mathrm{n} J_{\mathrm{n}} J'_{\mathrm{n}+1}}{D_{\mathrm{n}}^{TE} D_{\mathrm{n}+1}^{TE^*}}\,. \tag{15b}$$

It is then straightforward to further simplify the summation of (15a) and (15b) and to convert the sums to $\sum_{\mathrm{n}=0}^{+\infty}$. Upon doing so, the force given by (7) is directly obtained.

#82201 - $15.00 USD Received 24 Apr 2007; revised 4 Jun 2007; accepted 6 Jun 2007; published 12 Jun 2007